Combined analysis of the $\pi^- p \to K^0\Lambda$, ηn reactions in a chiral quark model

Li-Ye Xiao, Fan Ouyang, Kai-Lei Wang, and Xian-Hui Zhong*
Department of Physics, Hunan Normal University, Changsha 410081, China;
Synergetic Innovation Center for Quantum Effects and Applications (SICQEA), Changsha 410081, China;
and Key Laboratory of Low-Dimensional Quantum Structures and Quantum Control of Ministry of Education, Changsha 410081, China
(Received 16 February 2016; revised manuscript received 4 July 2016; published 2 September 2016)

A combined analysis of the reactions $\pi^- p \to K^0\Lambda$ and ηn is carried out with a chiral quark model. The data in the center-of-mass (c.m.) energy range from threshold up to $W \simeq 1.8$ GeV are reasonably described. For $\pi^- p \to K^0\Lambda$, it is found that $N(1535)S_{11}$ and $N(1650)S_{11}$ play crucial roles near threshold. The $N(1650)S_{11}$ resonance contributes to the reaction through configuration mixing with $N(1535)S_{11}$. The constructive interference between $N(1535)S_{11}$ and $N(1650)S_{11}$ is responsible for the peak structure around threshold in the total cross section. The n-pole, u-, and t-channel backgrounds provide significant contributions to the reaction as well. For the $\pi^- p \to \eta n$ process, the "first peak" in the total cross section is dominated by $N(1535)S_{11}$, which has a sizeable destructive interference with $N(1650)S_{11}$. Around $P_\pi \simeq 1.0\,\text{GeV}/c$ ($W \simeq 1.7$ GeV), there seems to be a small bump structure in the total cross section, which might be explained by the interference between the u channel and $N(1650)S_{11}$. The $N(1520)D_{13}$ resonance affects the angle distributions of the cross sections notably, although no obvious effects are seen in the total cross section. The role of P-wave state $N(1720)P_{13}$ should be further confirmed by future experiments. If $N(1720)P_{13}$ has a narrow width of $\Gamma \simeq 120$ MeV as found in our previous work by a study of the π^0 photoproduction processes, obvious evidence should be seen in the $\pi^- p \to K^0\Lambda$ and ηn processes as well. Finally, we give our predictions of the s-channel isospin-$\frac{1}{2}$ resonance contributions to the $\pi N \to \pi N$ reactions.

DOI: 10.1103/PhysRevC.94.035202

I. INTRODUCTION

Understanding the baryon spectrum and searching for the missing nucleon resonances and new exotic states are favored topics in hadronic physics [1]. Pion-nucleon (πN) scattering provides us an important tool to study the light baryon spectrum. Most of our current knowledge about the nucleon resonances listed in the Review of Particle Physics by the Particle Data Group (PDG) [2] was extracted from partial wave analyses of the πN scattering. As we know, in the constituent quark model a rich spectrum of nucleon resonances is predicted [3–5]; however, some of them are still missing. To look for the missing resonances and deal with the unresolved issues in hadronic physics, more precise measurements of pion-induced reactions were suggested recently in Ref. [6], meanwhile, reliable partial wave analyses are the same important as the precise measurements for us to extract the information on resonance properties.

In the πN scattering, the $\pi^- p \to K^0\Lambda$ and ηn reactions are especially interesting in hadronic physics. The reasons are as follows. (i) Only the baryon resonances with isospin $I = 1/2$ contribute to these two reactions due to the isospin selection rule. Thus, both $\pi^- p \to K^0\Lambda$ and ηn processes provide us a rather clear place to extract the properties of nucleon resonances without interferences from the Δ^* states. (ii) The $\pi^- p \to K^0\Lambda$ and ηn reactions can let us obtain information on strong couplings of nucleon resonances to $K\Lambda$ and ηN channels, which cannot be obtained in the elastic πN scattering. (iii) Furthermore, in these reactions one may find evidence of some resonances which couple only weakly to the πN channel. Hence, many studies about these two reactions have been carried out.

In experiments, some measurements of the $\pi^- p \to K^0\Lambda$ and ηn reactions were carried out about 20 or 30 years ago, the data had been collected in [7]. For the $\pi^- p \to K^0\Lambda$ reaction, the data of total cross section and differential cross sections can be obtained in the whole resonance range [8–15], furthermore, some data of Λ polarization are also obtained in the energy region $W < 1.8$ GeV [11]. For the $\pi^- p \to \eta n$ reaction, a few precise data on the differential cross sections and total cross section can be obtained near the $N(1535)S_{11}$ mass threshold from the Crystal Ball spectrometer at Brookhaven National Laboratory (BNL) [16]; however, other old data [17–22] might be problematic over the whole energy range due to limited angle coverage and uncontrollable uncertainties [23]. Thus, to get reliable information on the resonance properties, a combined analysis of the $\pi^- p \to K^0\Lambda$ and ηn reactions is necessary before new precise data are obtained.

Various theoretical approaches have been applied to analyze the $\pi^- p \to K^0\Lambda$ and/or ηn reactions, such as the chiral unitary model [24], K-matrix methods [25–35], dynamical coupled-channel models [7,36–41], the BnGa approach [42], chiral quark model [43,44], and other effective approaches [45–47]. However, the analyses from different models claim a different resonance content in the reactions [6]. For example, in the $\pi^- p \to K^0\Lambda$ reaction the large peak near $W = 1.7$ GeV is explained as the dominant contributions from both $N(1650)S_{11}$ and $N(1710)P_{11}$ in Ref. [25], from $N(1720)P_{13}$ in Ref. [27], or from $N(1535)S_{11}$, $N(1650)S_{11}$, and $N(1720)P_{13}$ in Ref. [45]. In the $\pi^- p \to \eta n$ reaction, the second bump structure near $W = 1.7$ GeV is explained as the dominant contribution of $N(1710)P_{11}$ in Refs. [7,27,29]; in Ref. [44] it is argued that this structure is mainly caused by $N(1720)P_{13}$; in Ref. [40,41] it is

*zhongxh@hunnu.edu.cn

suggested that this structure is due to the interference between $N(1535)S_{11}$ and $N(1650)S_{11}$. To clarify these puzzles in the reactions, more theoretical studies are needed.

In this work, we carry out a combined study of the $\pi^- p \to K^0\Lambda$ and ηn reactions within a chiral quark model. First, we hope to obtain a better understanding of the reaction mechanism for these reactions. In our previous work [43], we first extended the chiral quark model to study of the $\pi^- p \to \eta n$ reaction, where we only obtained reasonable results near threshold. In order to further understand the reaction in a higher resonance region and get more solid predictions, we need to revisit this reaction by combining with the reaction $\pi^- p \to K^0\Lambda$. Second, we expect to further confirm the extracted properties of $N(1535)S_{11}$ from the η- and π-meson photoproduction processes in our previous works [48,49]. Therein, we predicted that $N(1535)S_{11}$ might be explained as a mixing three-quark state between representations of $[70,^2 8]$ and $[70,^4 8]$ in the quark model. However, in the literature it is argued that $N(1535)S_{11}$ may contain a large admixture of pentaquark component for its large couplings to ηN and $K\Lambda$ channels [50,51]. Furthermore, the $N(1535)S_{11}$ resonance is also considered as a dynamically generated state in the chiral unitary models [52–55]. Finally, we hope to extract some information on $N(1720)P_{13}$ in the $\pi^- p \to K^0\Lambda$ and ηn reactions and test its properties obtained by us in the π-meson photoproduction processes, where we found that the $N(1720)P_{13}$ resonance might favor a narrow width of $\Gamma \simeq 120$ MeV [49], which is about a factor of 2 narrower than the world average value from PDG [2].

In the chiral quark model, an effective chiral Lagrangian is introduced to account for the quark-pseudoscalar-meson coupling. Since the quark-meson coupling is invariant under the chiral transformation, some of the low-energy properties of QCD are retained. There are several outstanding features for this model [43]. One is that only a very limited number of adjustable parameters will appear in this framework. In particular, only one overall parameter is needed for the nucleon resonances to be coupled to the pseudoscalar mesons in the SU(6)⊗O(3) symmetry limit. This is distinguished from hadronic models where each resonance requires one additional coupling constant as free parameter. Another one is that all the nucleon resonances can be treated consistently in the quark model. Thus, our model predictive power will be improved, and the extracted information of the resonance structures will be more reliable when we analyze the data. The chiral quark model has been well developed and widely applied to meson photoproduction reactions [48,49,56–68]. Recently, this model has been successfully extended to πN and KN reactions as well [43,69–71].

This work is organized as follows. The model is reviewed in Sec. II. Then, in Sec. III, our numerical results and analyses are presented and discussed. Finally, a summary is given in Sec. IV.

II. FRAMEWORK

In this section, we give a brief review of the chiral quark model. In this model, the s- and u-channel transition amplitudes can be expressed as [43]

$$\mathcal{M}_s = \sum_j \langle N_f|H_m^f|N_j\rangle\langle N_j|\frac{1}{E_i+\omega_i-E_j}H_m^i|N_i\rangle, \quad (1)$$

$$\mathcal{M}_u = \sum_j \langle N_f|H_m^i\frac{1}{E_i-\omega_i-E_j}|N_j\rangle\langle N_j|H_m^f|N_i\rangle, \quad (2)$$

where H_m^i and H_m^f stand for the incoming and outgoing meson-quark couplings, respectively. They might be described by the effective chiral Lagrangian [59,60]

$$H_m = \frac{1}{f_m}\bar{\psi}_j\gamma_\mu^j\gamma_5^j\psi_j\vec{\tau}\cdot\partial^\mu\vec{\phi}_m, \quad (3)$$

where ψ_j represents the jth quark field in a hadron, f_m is the meson's decay constant, and ϕ_m is the field of the pseudoscalar-meson octet. The ω_i and ω_f are the energies of the incoming and outgoing mesons, respectively. $|N_i\rangle$, $|N_j\rangle$, and $|N_f\rangle$ stand for the initial, intermediate, and final states, respectively, and their corresponding energies are E_i, E_j, and E_f, which are the eigenvalues of the nonrelativistic Hamiltonian of the constituent quark model $\hat{H}$ [3,4]. The s- and u-channel transition amplitudes have been worked out in the harmonic oscillator basis in Refs. [43,70,71], and the g factors appearing in the s- and u-channel amplitudes have been defined in Ref. [70], whose values are worked out and listed in Table I.

TABLE I. g factors extracted in the symmetric quark model.

Factor	$\pi^- p \to K^0\Lambda$	$\pi^- p \to \eta n$
g_{s1}	$\frac{\sqrt{6}}{2}$	1.0
g_{s2}	$\frac{\sqrt{6}}{3}$	$\frac{2}{3}$
g_{v1}	$\frac{\sqrt{6}}{2}$	$\frac{5}{3}$
g_{v2}	$\frac{\sqrt{6}}{3}$	0.0
g_{s1}^u	0.0	1.0
g_{s2}^u	$\frac{\sqrt{6}}{3}$	$\frac{2}{3}$
g_{v1}^u	0.0	$\frac{5}{3}$
g_{v2}^u	$-\frac{\sqrt{6}}{3}$	0.0
g_t^s	$\frac{\sqrt{6}}{2}$	1.0
g_t^v	$\frac{\sqrt{6}}{2}$	$\frac{5}{3}$

The t-channel contributions of vector and/or scalar exchanges are included in this work. The vector meson-quark and scalar meson-quark couplings are given by

$$H_V = \bar{\psi}_j\left(a\gamma^\nu + \frac{b\sigma^{\nu\lambda}\partial_\lambda}{2m_q}\right)V_\nu\psi_j, \quad (4)$$

$$H_S = g_{Sqq}\bar{\psi}_j\psi_j S, \quad (5)$$

where V and S stand for the vector and scalar fields, respectively. The constants a, b, and g_{Sqq} are vector, tensor, and scalar coupling constants, respectively. They are treated as free parameters in this work.

Meanwhile, the VPP and SPP couplings (P stands for a pseudoscalar-meson) are adopted as

$$H_{VPP} = -iG_V \mathrm{Tr}([\phi_m, \partial_\mu \phi_m] V^\mu), \quad (6)$$

$$H_{SPP} = \frac{g_{SPP}}{2m_\pi} \partial_\mu \phi_m \partial^\mu \phi_m S, \quad (7)$$

where G_V and g_{SPP} are the VPP and SPP coupling constants, respectively. They will be determined by the experimental data.

The t-channel transition amplitude has been given in Ref. [71]. In this work, the scalar κ-meson and vector K^*-meson exchanges are considered for the $\pi^- p \to K^0 \Lambda$ process, while

TABLE II. The s-channel resonance amplitudes within $n = 2$ shell for the $\pi^- p \to K^0\Lambda, \eta n$ processes. We have defined $M_S \equiv [\frac{\omega_i}{\mu_q} - |\mathbf{A}_{\rm in}|\frac{2|\mathbf{k}|}{3\alpha^2}][\frac{\omega_f}{\mu_q} - |\mathbf{A}_{\rm out}|\frac{2|\mathbf{q}|}{3\alpha^2}]$, $M_P = M_D \equiv \frac{|\mathbf{A}_{\rm out}||\mathbf{A}_{\rm in}|}{|\mathbf{k}||\mathbf{q}|}$, $M_{P0} \equiv [\frac{\omega_i}{\mu_q} - |\mathbf{A}_{\rm in}|\frac{|\mathbf{k}|}{\alpha^2}][\frac{\omega_f}{\mu_q} - |\mathbf{A}_{\rm out}|\frac{|\mathbf{q}|}{\alpha^2}]$, $M_{P2} \equiv [\frac{\omega_i}{\mu_q} - |\mathbf{A}_{\rm in}|\frac{2|\mathbf{k}|}{5\alpha^2}][\frac{\omega_f}{\mu_q} - |\mathbf{A}_{\rm out}|\frac{2|\mathbf{q}|}{5\alpha^2}]$, $M_F \equiv |\mathbf{A}_{\rm out}||\mathbf{A}_{\rm in}|\frac{|\mathbf{k}||\mathbf{q}|}{\alpha^4}$, $P_l'(z) \equiv \frac{\partial P_l(z)}{\partial z}$, $X_{S1} \equiv [\cos\theta_S + \sin\theta_S][2\cos\theta_S - \sin\theta_S]$, and $X_{S2} \equiv [\sin\theta_S - \cos\theta_S][2\sin\theta_S + \cos\theta_S]$. The functions $\mathbf{A}_{\rm in}$ and $\mathbf{A}_{\rm out}$ have been defined in [71]. The μ_q is a reduced mass at the quark level, which equals $1/\mu_q = 1/m_u + 1/m_s$ for K productions, while $1/\mu_q = 2/m_u$ for η productions. $P_l(z)$ is the Legendre function with $z = \cos\theta$.

$[N_6, {}^{2S+1}N_3, n, l]$	$l_{2I,2J}$	$\mathcal{O}_R$	$\pi^- p \to K^0\Lambda$	$\pi^- p \to \eta n$
$\|70,{}^2 8,0,0\rangle$	$P_{11}(n)$	$f(\theta)$	$\frac{5}{\sqrt{6}} M_P \mathbf{\|k\|\|q\|} P_1(z)$	$\frac{5}{3} M_P \mathbf{\|k\|\|q\|} P_1(z)$
		$g(\theta)$	$\frac{5}{\sqrt{6}} M_P \mathbf{\|k\|\|q\|} \sin\theta P_1'(z)$	$\frac{5}{3} M_P \mathbf{\|k\|\|q\|} \sin\theta P_1'(z)$
$+\cos\theta_S \|70,{}^2 8,1,1\rangle$	$N(1535)S_{11}$	$f(\theta)$	$\frac{\sqrt{6}}{12} \cos^2\theta_S M_S \alpha^2$	$\frac{1}{6} X_{S1} M_S \alpha^2$
$-\sin\theta_S \|70,{}^4 8,1,1\rangle$		$g(\theta)$		
$+\cos\theta_S \|70,{}^4 8,1,1\rangle$	$N(1650)S_{11}$	$f(\theta)$	$\frac{\sqrt{6}}{12} \sin^2\theta_S M_S \alpha^2$	$\frac{1}{6} X_{S2} M_S \alpha^2$
$+\sin\theta_S \|70,{}^2 8,1,1\rangle$		$g(\theta)$		
$\|70,{}^2 8,1,1\rangle$	$N(1520)D_{13}$	$f(\theta)$	$\frac{20\sqrt{6}}{27} M_D \frac{\mathbf{\|k\|^2\|q\|^2}}{\alpha^2} P_2(z)$	$\frac{76}{135} M_D \frac{\mathbf{\|k\|^2\|q\|^2}}{\alpha^2} P_2(z)$
		$g(\theta)$	$\frac{10\sqrt{6}}{27} M_D \frac{\mathbf{\|k\|^2\|q\|^2}}{\alpha^2} \sin(\theta) P_2'(z)$	$\frac{38}{135} M_D \frac{\mathbf{\|k\|^2\|q\|^2}}{\alpha^2} \sin\theta P_2'(z)$
$\|70,{}^4 8,1,1\rangle$	$N(1700)D_{13}$	$f(\theta)$		$-\frac{38}{1350} M_D \frac{\mathbf{\|k\|^2\|q\|^2}}{\alpha^2} P_2(z)$
		$g(\theta)$		$-\frac{19}{1350} M_D \frac{\mathbf{\|k\|^2\|q\|^2}}{\alpha^2} \sin\theta P_2'(z)$
	$N(1675)D_{15}$	$f(\theta)$		$-\frac{2}{15} M_D \frac{\mathbf{\|k\|^2\|q\|^2}}{\alpha^2} P_2(z)$
		$g(\theta)$		$\frac{2}{45} M_D \frac{\mathbf{\|k\|^2\|q\|^2}}{\alpha^2} \sin\theta P_2'(z)$
$\|56,{}^2 8,2,0\rangle$	$N(1440)P_{11}$	$f(\theta)$	$\frac{5\sqrt{6}}{24\times 27} M_{P0} \mathbf{\|k\|\|q\|} P_1(z)$	$\frac{5}{12\times 27} M_{P0} \mathbf{\|k\|\|q\|} P_1(z)$
		$g(\theta)$	$\frac{5\sqrt{6}}{24\times 27} M_{P0} \mathbf{\|k\|\|q\|} \sin\theta P_1'(z)$	$\frac{5}{12\times 27} M_{P0} \mathbf{\|k\|\|q\|} \sin\theta P_1'(z)$
$\|70,{}^2 8,2,0\rangle$	$N(1710)P_{11}$	$f(\theta)$	$\frac{2\sqrt{6}}{24\times 27} M_{P0} \mathbf{\|k\|\|q\|} P_1(z)$	$\frac{1}{3\times 27} M_{P0} \mathbf{\|k\|\|q\|} P_1(z)$
		$g(\theta)$	$\frac{2\sqrt{6}}{24\times 27} M_{P0} \mathbf{\|k\|\|q\|} \sin\theta P_1'(z)$	$\frac{1}{3\times 27} M_{P0} \mathbf{\|k\|\|q\|} \sin\theta P_1'(z)$
$\|70,{}^4 8,2,2\rangle$	$N(1880)P_{11}$	$f(\theta)$		$-\frac{5}{4\times 81} M_{P2} \mathbf{\|k\|\|q\|} P_1(z)$
		$g(\theta)$		$-\frac{5}{4\times 81} M_{P2} \mathbf{\|k\|\|q\|} \sin\theta P_1'(z)$
$\|70,{}^4 8,2,0\rangle$	$N(?)P_{13}$	$f(\theta)$		$-\frac{1}{2\times 81} M_{P0} \mathbf{\|k\|\|q\|} P_1(z)$
		$g(\theta)$		$\frac{1}{4\times 81} M_{P0} \mathbf{\|k\|\|q\|} \sin\theta P_1'(z)$
$\|56,{}^2 8,2,2\rangle$	$N(1720)P_{13}$	$f(\theta)$	$\frac{25\sqrt{6}}{24\times 27} M_{P2} \mathbf{\|k\|\|q\|} P_1(z)$	$\frac{25}{4\times 81} M_{P2} \mathbf{\|k\|\|q\|} P_1(z)$
		$g(\theta)$	$-\frac{25\sqrt{6}}{48\times 27} M_{P2} \mathbf{\|k\|\|q\|} \sin\theta P_1'(z)$	$-\frac{25}{8\times 81} M_{P2} \mathbf{\|k\|\|q\|} \sin\theta P_1'(z)$
$\|70,{}^2 8,2,2\rangle$	$N(1900)P_{13}$	$f(\theta)$	$\frac{10\sqrt{6}}{24\times 27} M_{P2} \mathbf{\|k\|\|q\|} P_1(z)$	$\frac{5}{81} M_{P2} \mathbf{\|k\|\|q\|} P_1(z)$
		$g(\theta)$	$-\frac{10\sqrt{6}}{48\times 27} M_{P2} \mathbf{\|k\|\|q\|} \sin\theta P_1'(z)$	$-\frac{5}{2\times 81} M_{P2} \mathbf{\|k\|\|q\|} \sin\theta P_1'(z)$
$\|70,{}^4 8,2,2\rangle$	$N(?)P_{13}$	$f(\theta)$		$-\frac{5}{4\times 81} M_{P2} \mathbf{\|k\|\|q\|} P_1(z)$
		$g(\theta)$		$\frac{5}{8\times 81} M_{P2} \mathbf{\|k\|\|q\|} \sin\theta P_1'(z)$
$\|56,{}^2 8,2,2\rangle$	$N(1680)F_{15}$	$f(\theta)$	$\frac{3\sqrt{6}}{4} M_F \mathbf{\|k\|\|q\|} P_3(z)$	$\frac{3}{2} M_F \mathbf{\|k\|\|q\|} P_3(z)$
		$g(\theta)$	$\frac{\sqrt{6}}{4} M_F \mathbf{\|k\|\|q\|} P_3'(z)$	$\frac{1}{2} M_F \mathbf{\|k\|\|q\|} \sin\theta P_3'(z)$
$\|70,{}^2 8,2,2\rangle$	$N(1860)F_{15}$	$f(\theta)$	$\frac{3\sqrt{6}}{10} M_F \mathbf{\|k\|\|q\|} P_3(z)$	$\frac{6}{5} M_F \mathbf{\|k\|\|q\|} P_3(z)$
		$g(\theta)$	$\frac{\sqrt{6}}{10} M_F \mathbf{\|k\|\|q\|} \sin\theta P_3'(z)$	$\frac{2}{5} M_F \mathbf{\|k\|\|q\|} \sin\theta P_3'(z)$
$\|70,{}^4 8,2,2\rangle$	$N(?)F_{15}$	$f(\theta)$		$-\frac{3}{35} M_F \mathbf{\|k\|\|q\|} P_3(z)$
		$g(\theta)$		$-\frac{1}{35} M_F \mathbf{\|k\|\|q\|} \sin\theta P_3'(z)$
$\|70,{}^4 8,2,2\rangle$	$N(?)F_{17}$	$f(\theta)$		$-\frac{18}{35} M_F \mathbf{\|k\|\|q\|} P_4(z)$
		$g(\theta)$		$\frac{9}{70} M_F \mathbf{\|k\|\|q\|} \sin\theta P_3'(z)$

the scalar $a_0(980)$-meson exchange is considered for the $\pi^- p \to \eta n$ process.

It should be pointed out that the amplitudes in terms of the harmonic oscillator principle quantum number n are sums of a set of SU(6) multiplets with the same n. To obtain the contributions of individual resonances, we need to separate out the single-resonances-excitation amplitudes within each principle number n in the s channel. Taking into account the width effects of the resonances, the resonance transition amplitudes of s channel can be generally expressed as [43,71]

$$\mathcal{M}_R^s = \frac{2M_R}{s - M_R^2 + iM_R\Gamma_R}\mathcal{O}_R e^{-(\mathbf{k}^2+\mathbf{q}^2)/6\alpha^2}, \tag{8}$$

where $\sqrt{s} = E_i + \omega_i$ is the total energy of the system; $\mathbf{k}$ and $\mathbf{q}$ stand for the momenta of incoming and outgoing mesons, respectively; α is the harmonic oscillator strength; $\mathcal{O}_R$ is the separated operators for individual resonances in the s channel; and M_R is the mass of the s-channel resonance with a width Γ_R. The transition amplitudes can be written in a standard form [72]:

$$\mathcal{O}_R = f(\theta) + ig(\theta)\boldsymbol{\sigma}\cdot\mathbf{n}, \tag{9}$$

where $\boldsymbol{\sigma}$ is the spin operator of the nucleon, while $\mathbf{n} \equiv \mathbf{q} \times \mathbf{k}/|\mathbf{k} \times \mathbf{q}|$. $f(\theta)$ and $g(\theta)$ stand for the non-spin-flip and spin-flip amplitudes, respectively, which can be expanded in terms of the familiar partial wave amplitudes $T_{l\pm}$ for the states with $J = l \pm 1/2$:

$$f(\theta) = \sum_{l=0}^{\infty}[(l+1)T_{l+} + lT_{l-}]P_l(\cos\theta), \tag{10}$$

$$g(\theta) = \sum_{l=0}^{\infty}[T_{l-} - T_{l+}]\sin\theta P_l'(\cos\theta), \tag{11}$$

where θ is the scattering angle between $\mathbf{k}$ and $\mathbf{q}$.

We have extracted the scattering amplitudes of the s-channel resonances within the $n = 2$ shell for both $\pi^- p \to K^0\Lambda$ and $\pi^- p \to \eta n$, which have been listed in Table II. It should be pointed out that the contributions of s-channel resonances with a $[70,^4 8]$ representation are forbidden in the $\pi^- p \to K^0\Lambda$ reaction due to the Moorhouse selection rule [73,74]. Comparing these amplitudes of different resonances with each other, one can easily find which states are the main contributors to the reactions in the SU(6)⊗O(3) symmetry limit.

Finally, the differential cross section $d\sigma/d\Omega$ and polarization of final baryon P can be calculated by

$$\frac{d\sigma}{d\Omega} = \frac{(E_i + M_i)(E_f + M_f)}{64\pi^2 s(2M_i)(2M_f)}\frac{|\mathbf{q}|}{|\mathbf{k}|}\frac{1}{2} \times \sum_{\lambda_i,\lambda_f}\left|M_{\lambda_f,\lambda_i}\right|^2,$$

$$P = 2\frac{\mathrm{Im}[f(\theta)g^*(\theta)]}{|f(\theta)|^2 + |g(\theta)|^2}, \tag{12}$$

where $\lambda_i = \pm\frac{1}{2}$ and $\lambda_f = \pm\frac{1}{2}$ are the helicities of the initial and final baryon states, respectively.

TABLE III. Various parameters used in this work. The label "fixed" after a parameter means this parameter is fixed in our calculations, while the label "fitted" after a parameter means this parameter is determined by fitting the data.

Constituent quark masses	m_u	330 MeV	fixed
	m_d	330 MeV	fixed
	m_s	450 MeV	fixed
Harmonic oscillator parameter	α	400 MeV	fixed
$n = 1,2$ shell degenerate resonance masses	M_1	1650 MeV	fixed
	M_2	1750 MeV	fixed
Coupling constants	$g_{a_0\pi\eta}g_{a_0NN}$	100	fixed
	$G_V a$	3.0 ± 1.5	fitted
	$g_{SPP}g_{Sqq}$	36.4 ± 5.0	fitted
	$g_{KN\Lambda}$	$6.87^{+0.04}_{-0.09}$	fitted
	$g_{\eta NN}$	2.50 ± 0.05	fitted
	$g_{\pi NN}$	13.48	fixed
Mixing angle	θ_S	$26.9^\circ \pm 1.0^\circ$	fitted

III. CALCULATION AND ANALYSIS

A. Parameters

The various parameters used in our calculations have been collected in Table III. The universal value of harmonic oscillator parameter α and constituent quark masses m_u, m_d, and m_s are fixed with $\alpha = 400$ MeV, $m_u = m_d = 330$ MeV, and $m_s = 450$ MeV, which are widely adopted and well determined in our previous quark model calculations.

In our work, the s-channel resonance transition amplitude, $\mathcal{O}_R$, is derived in the SU(6)⊗O(3) symmetric quark model limit. In reality, the symmetry of SU(6)⊗O(3) is generally broken due to, e.g., spin-dependent forces in the quark-quark interaction. As a result, configuration mixing would occur, which can produce an effect on our theoretical predictions. According to our previous studies of the η and π^0 photoproduction on the nucleons [48,49], we found the configuration mixings seem to be inevitable for the low-lying S-wave nucleon resonances $N(1535)S_{11}$ and $N(1650)S_{11}$. Thus, in this work we also consider configuration mixing effects in the S-wave states and use the same mixing scheme as in our previous works [48,49],

$$\begin{pmatrix} S_{11}(1535) \\ S_{11}(1650) \end{pmatrix} = \begin{pmatrix} \cos\theta_S & -\sin\theta_S \\ \sin\theta_S & \cos\theta_S \end{pmatrix}\begin{pmatrix} |70,^2 8,1/2^-\rangle \\ |70,^4 8,1/2^-\rangle \end{pmatrix}, \tag{13}$$

where θ_S is the mixing angle. Then, the s-channel resonance transition amplitudes of the S-wave states $N(1535)S_{11}$ and $N(1650)S_{11}$ are related to the mixing angle θ_S. These transition amplitudes have been worked out and listed in Table II. The mixing angle θ_S has been determined by fitting the data. The determined value $\theta_S \simeq 26.9^\circ$ is consistent with that obtained in our previous works [48,49].

In the calculations, the quark–pseudoscalar-meson couplings are the overall parameters in the s- and u-channel transitions. However, they are not totally free ones. They can be related to the hadronic couplings via the Goldberger-Treiman

relation [75]

$$g_{mBB'} = \frac{g_A^m M_N}{F_m}, \tag{14}$$

where m stands for the pseudoscalar mesons, η, π, and K; B and B' stand for the baryons in the initial and final states, respectively; g_A^m is the axial vector coupling for the meson; and F_m is the meson decay constant, which can be related to f_m defined earlier by $F_m = f_m/\sqrt{2}$.

It should be pointed out that the πNN coupling constant $g_{\pi NN}$ is a well-determined number, $g_{\pi NN} = 13.48$; thus, we fix it in our calculations. For the other two coupling constants, $g_{KN\Lambda}$ and $g_{\eta NN}$, there are larger uncertainties. Thus, we determine them by fitting the data of the $\pi^- p \to K^0\Lambda, \eta n$ processes, respectively. We get that

$$g_{KN\Lambda} \simeq 6.87, \quad g_{\eta NN} \simeq 2.50. \tag{15}$$

The coupling constant $g_{\eta NN}$ extracted in present work is consistent with that extracted from the η meson photoproduction on nucleons in our previous work [48], and also is in good agreement with the determinations in Refs. [58,76–78]. The coupling constant $g_{KN\Lambda}$ extracted by us is consistent with that extracted from the K-meson photoproduction on nucleons in Refs. [37,57,79].

In the t channel of the $\pi^- p \to K^0\Lambda$ process, there are two free parameters, $G_V a$ and $g_{SPP} g_{Sqq}$, which come from K^* and κ exchanges, respectively. By fitting the data, we get $G_V a \simeq 3.0$ and $g_{SPP} g_{Sqq} \simeq 36.4$, which are close to our previous determinations in the $K^- p$ scattering [71]. In the t channel of the $\pi^- p \to \eta n$ process, the parameter from the a_0 exchange $g_{a_0\pi\eta} g_{a_0 NN}$ is adopted at the often used value $g_{a_0\pi\eta} g_{a_0 NN} \simeq 100$ in Refs. [36,80], because our calculations are less sensitive to it.

In the u channel, it is found that contributions from the $n \geqslant 1$ shell resonances are negligibly small and insensitive to their masses. Thus, the $n = 1$ and the $n = 2$ shell resonances are treated as degeneration. In the calculations, we take $M_1 = 1650$ MeV ($M_2 = 1750$ MeV) for the degenerate mass of $n = 1$ ($n = 2$) shell resonances.

In the s channel, the masses and widths of the nucleon resonances are taken from the PDG [2] or the constituent quark model predictions [5] if no experimental data are available. For the main resonances $N(1535)S_{11}$, $N(1650)S_{11}$, and $N(1520)D_{13}$, we allow their masses and widths to change in a proper range in order to better describe the data. The determined values are listed in Table IV. It is found that the main resonance masses and widths extracted by us are in good agreement with the world average values from PDG [2]. One point should be emphasized: our global fits of the $\pi^- p \to \eta n, K^0\Lambda$ reaction data seem to favor a broad width $\Gamma \gtrsim 200$ MeV for $N(1720)P_{13}$; however, this width is much broader than $\Gamma \simeq 120$ MeV extracted from the neutral pion photoproduction processes in our previous work [49]. A similar narrow width for $N(1720)P_{13}$ was also found by the CLAS Collaboration in the reaction $ep \to ep'\pi^+\pi^-$ [81]. We will further discuss whether a narrow width state $N(1720)P_{13}$ is allowed or not in the $\pi^- p \to \eta n, K^0\Lambda$ reactions later.

Combining the extracted coupling constants, $g_{KN\Lambda}$ and $g_{\eta NN}$, and resonance masses, we further determine some partial width ratios of the main contributors $N(1535)S_{11}$ and $N(1650)S_{11}$ to the reactions, which have been listed in Table V. Form the table we can see that the partial width ratios $\Gamma_{\eta N}/\Gamma_{\pi N}$ and $\Gamma_{K\Lambda}/\Gamma_{\pi N}$ determined by us are close to the upper limit of the values from the PDG [2].

TABLE IV. Resonance masses M_R (MeV) and widths Γ_R (MeV) in this work compared with the world average value from the PDG [2]. The resonance parameters of $N(1535)S_{11}$, $N(1535)S_{11}$, and $N(1520)D_{13}$ are determined by fitting the data. The other resonance parameters are fixed in our calculations because the results are less sensitive to them.

Resonance	M_R	Γ_R	M_R (PDG)	Γ_R (PDG)
$N(1535)S_{11}$	1524^{+6}_{-7}	124^{+12}_{-3}	1535 ± 10	150 ± 25
$N(1650)S_{11}$	1670^{+16}_{-24}	107 ± 30	1655^{+15}_{-10}	140 ± 30
$N(1520)D_{13}$	1515 ± 20	125 ± 20	1515 ± 5	115^{+10}_{-15}
$N(1700)D_{13}$	1700	150	1700 ± 50	150^{+100}_{-50}
$N(1675)D_{15}$	1685	140	1675 ± 5	150^{+15}_{-20}
$N(1440)P_{11}$	1430	350	1430 ± 20	350 ± 100
$N(1710)P_{11}$	1710	200	1710 ± 30	100^{+150}_{-50}
$N(1870)P_{11}$	1870	235	1870 ± 35	235 ± 65
$N(?)P_{13}$	2000	200		
$N(1720)P_{13}$	1690	400	1720^{+30}_{-20}	250^{+150}_{-100}
$N(1900)P_{13}$	1900	250	~ 1900	~ 250
$N(?)P_{13}$	2040	200		
$N(1680)F_{15}$	1680	130	1685 ± 5	130 ± 10
$N(1860)F_{15}$	1860	270	1860^{+100}_{-40}	270^{+140}_{-50}
$N(?)F_{15}$	2050	200		
$N(?)F_{17}$	1990	200		

It should be pointed out that all adjustable parameters are determined by globally fitting the measured differential cross sections of the $\pi^- p \to \eta n, K^0\Lambda$ processes. All the data sets used in our fits have been shown in Figs. 3 and 5. The reduced χ^2 per data point obtained in our fits has been listed in Table VI. To clearly see the role of one component in the reactions, the χ^2's with one resonance or one background switched off are also given in the table.

Finally, to know some uncertainties of the parameter determined by us we vary it around its central value until the predictions are inconsistent with the data within their uncertainties. The obtained uncertainties for these parameters have been given in Tables III and IV.

B. $\pi^- p \to K^0\Lambda$

The differential cross sections and total cross section of the $\pi^- p \to K^0\Lambda$ process compared with experimental data are

TABLE V. Extracted partial decay width ratios for $N(1535)$ and $N(1650)$ resonances compared with the values from the PDG [2].

Resonance	$\frac{\Gamma_{\eta N}}{\Gamma_{\pi N}}$ (ours)	$\frac{\Gamma_{\eta N}}{\Gamma_{\pi N}}$ (PDG)	$\frac{\Gamma_{K\Lambda}}{\Gamma_{\pi N}}$ (ours)	$\frac{\Gamma_{K\Lambda}}{\Gamma_{\pi N}}$ (PDG)
$N(1535)S_{11}$	1.57 ± 0.06	$1.20^{+0.29}_{-0.62}$		
$N(1650)S_{11}$	0.23 ± 0.01	0.05–0.30	$0.20^{+0.003}_{-0.005}$	0.03–0.22

TABLE VI. Reduced χ^2 per data point of the full model and that with one resonance or one background switched off obtained in a global fit of the data of $\pi^- p \to K^0\Lambda$ and $\pi^- p \to \eta n$. The corresponding partial $\chi^2 s$ for the $\pi^- p \to K^0\Lambda$ (labeled with χ^2_K) and $\pi^- p \to \eta n$ (labeled with χ^2_η) are also included.

	Full model	n-pole	$N(1535)S_{11}$	$N(1650)S_{11}$	$N(1520)D_{13}$	$N(1720)P_{13}$	u-channel	t-channel
χ^2	5.98	14.96	265.03	24.88	14.53	5.99	15.79	15.03
χ^2_η	8.54	13.36	466.86	40.31	24.52	8.07	18.09	10.49
χ^2_K	2.78	16.95	12.75	5.58	2.05	3.39	12.92	20.70

shown in Figs. 1 and 2, respectively. From these figures, it is found that the experimental data in the c.m. energy range from threshold up to $W \simeq 1.8$ GeV are reasonably described within the chiral quark model.

Obvious roles of the S-wave states $N(1535)S_{11}$ and $N(1650)S_{11}$ are seen in the reaction. The constructive interferences between $N(1535)S_{11}$ and $N(1650)S_{11}$ are crucial to reproduce the bump structure near threshold in the total cross section. Switching off the contributions of $N(1535)S_{11}$ or $N(1650)S_{11}$, the cross sections around their mass thresholds are notably underestimated (see Figs. 2 and 3). It should be pointed out that, in the symmetric quark model, the $N(1650)S_{11}$ resonance corresponds to the [70,^{4}8] representation. In the SU(6)⊗O(3) symmetry limit, the contributions of $N(1650)S_{11}$ should be forbidden in the $\pi^- p \to K^0\Lambda$ reaction due to the Moorhouse selection rule [73,74]. The obvious role of $N(1650)S_{11}$ in the $\pi^- p \to K^0\Lambda$ reaction further confirms that the SU(6)⊗O(3) symmetry is broken, and the configuration mixing between $N(1535)S_{11}$ and $N(1650)S_{11}$ should be necessary as suggested in our previous studies of the meson photoproduction processes [48,49].

Furthermore, some contributions from $N(1720)P_{13}$ might be seen in the differential cross sections. At backward angles, the differential cross sections are slightly underestimated without its contribution. For the large uncertainties of the data, here we cannot obtain solid information on $N(1720)P_{13}$. If we adopt a narrow width $\Gamma \simeq 120$ MeV as suggested in our previous work [49], from Fig. 8 we see that the peak of the bump structure in the total cross section becomes sharper, and around the mass threshold of $N(1720)P_{13}$ the differential cross sections at forward angles are enhanced significantly. Our theoretical predictions with a narrow width for $N(1720)P_{13}$ are

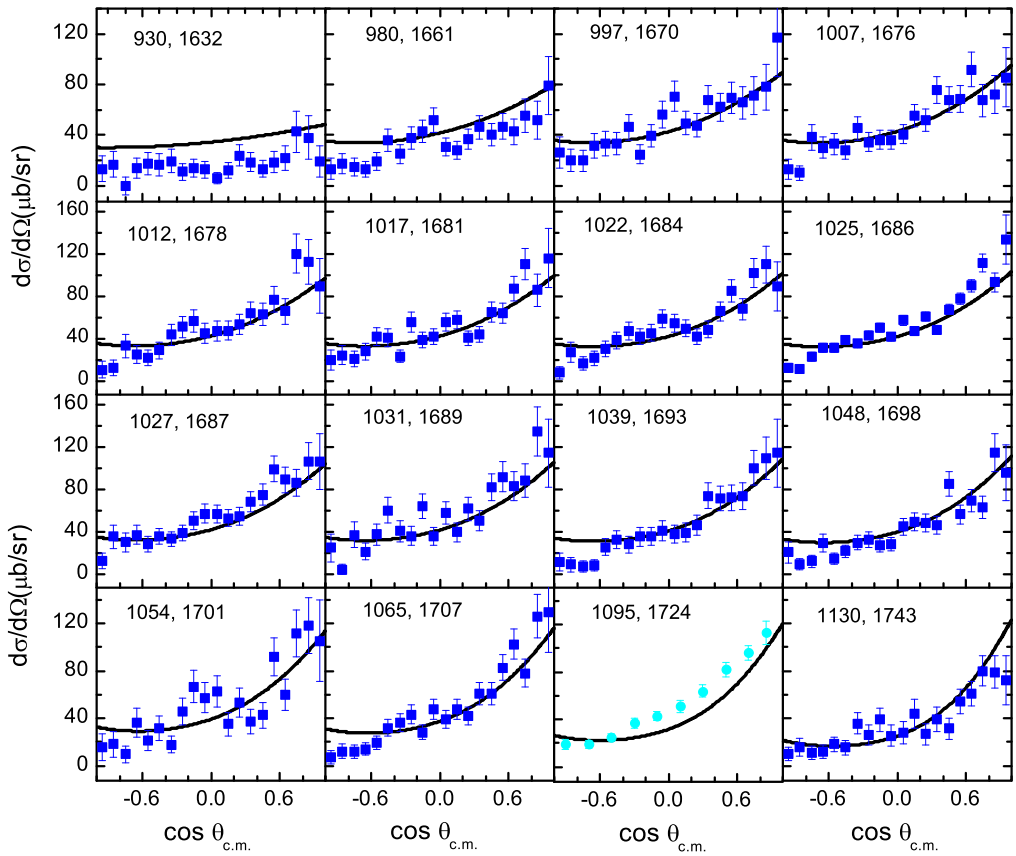

FIG. 1. Differential cross sections of the reaction $\pi^- p \to K^0\Lambda$ compared with the experimental data from Refs. [14] (solid squares) and [11] (solid circle). The first and second numbers in each figure correspond to the π^- beam momentum P_π (MeV/c) and the πN center-of-mass (c.m.) energy W (MeV), respectively.

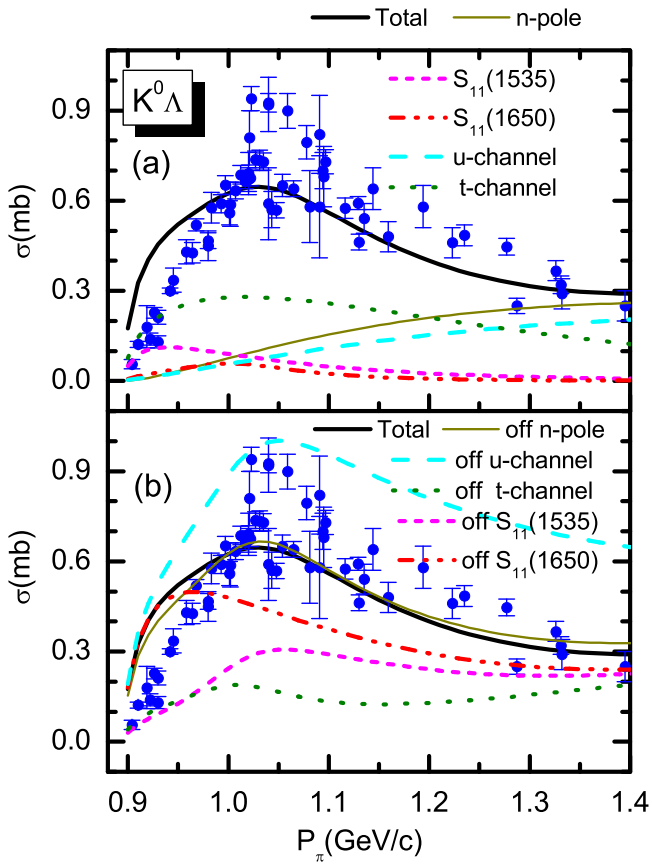

FIG. 2. Total cross section of the reaction $\pi^- p \to K^0\Lambda$ compared with experimental data from Ref. [15]. The bold solid curves correspond to the full model result. In (a), exclusive cross sections for $S_{11}(1535)$, $S_{11}(1650)$, nucleon pole, u channel, and t channel are indicated explicitly by the legends. In (b), the results by switching off the contributions of $S_{11}(1535)$, $S_{11}(1650)$, nucleon pole, u channel, and t channel are indicated explicitly by the legends.

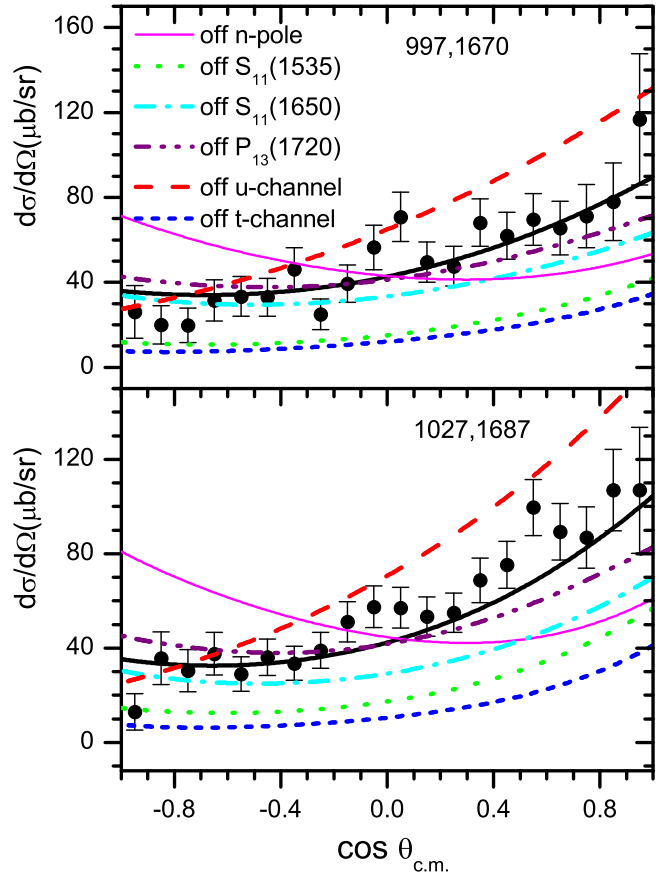

FIG. 3. Differential cross sections of the reaction $\pi^- p \to K^0\Lambda$ compared with experimental data [14] at two energy points $P_\pi =$ 997,1027 MeV/c. The bold solid curves correspond to the full model result. The predictions by switching off the contributions from $N(1535)S_{11}$, $N(1650)S_{11}$, $N(1720)P_{13}$, and n-pole, u-, and t-channel backgrounds are indicated explicitly by the legends in the figures.

still consistent with the data within their uncertainties. Thus, to finally determine the properties of $N(1720)P_{13}$, we need more accurate measurements of the $\pi^- p \to K^0\Lambda$ reaction.

The n-pole, u-, and t-channel backgrounds play crucial roles in the reaction as well. From Figs. 2 and 3, one can see that by switching off the u-channel contribution, the cross sections should be strongly overestimated, while by switching off the t-channel contribution, the cross sections will be underestimated notably. The n pole has obvious effects on angle distributions of the cross sections in the whole energy region what we considered. Without the n pole contribution, the differential cross sections at forward angles should be notably underestimated, while those at backward angles should be notably overestimated.

In experiments, there are some old measurements for the Λ polarization of the $\pi^- p \to K^0\Lambda$ reaction [11]. In Fig. 4 we compare our chiral quark model predictions with the observations in the c.m. energy range $W < 1.8$ GeV. We found that the experimental observations can be explained reasonably. It should be emphasized that our theoretical calculations seem to slightly underestimate the Λ polarization. This phenomenon also exist in the coupled-channel approach calculations [7]. Improved measurements and more reliable experimental data of the polarization are needed to clarify the discrepancies.

As a whole, obvious evidence of $N(1535)S_{11}$ and $N(1650)S_{11}$ is found in the $\pi^- p \to K^0\Lambda$ reaction, which is consistent with the recent analysis within an effective Lagrangian approach [45]. It should be emphasized that the $N(1650)S_{11}$ resonance contributes to the reaction via the configuration mixing with $N(1535)S_{11}$. The determined mixing angle is $\theta_S \simeq 26.9^\circ$. Furthermore, remarkable contributions from the backgrounds, n pole, u, and t channels are found in the reaction. There might be sizable contributions from $N(1720)P_{13}$; the present data cannot determine whether it is a narrow or broad state. No clear evidence from the other nucleon resonances, such as $N(1520)D_{13}$, $N(1700)D_{13}$, and $N(1710)P_{11}$, is found in the reaction. Finally, it should be mentioned that $N(1710)P_{11}$ was considered as one of the main contributors to $\pi^- p \to K^0\Lambda$ in the literature [7,25,47], which is in disagreement with our prediction and that from Refs. [27,28,45].

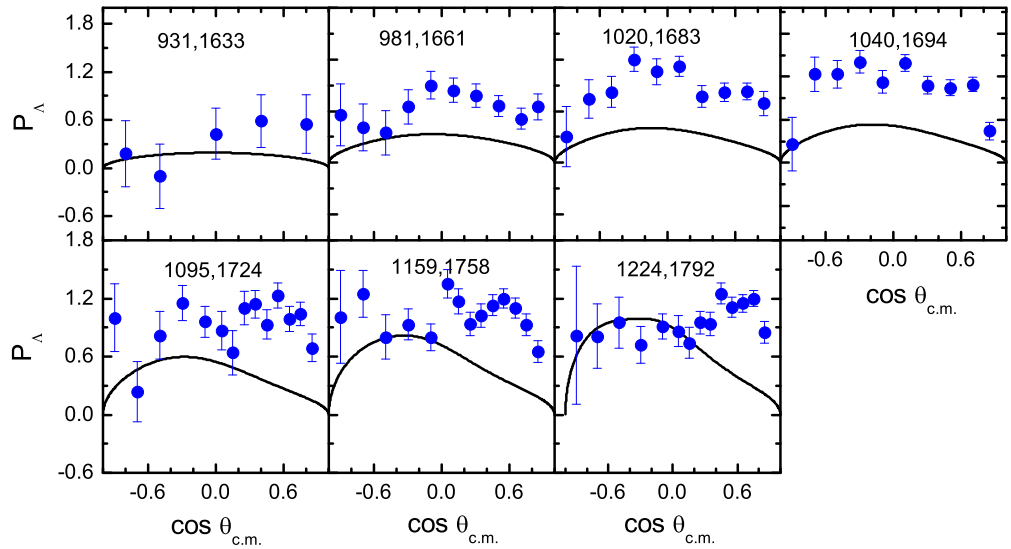

FIG. 4. Λ polarization of the $\pi^- p \to K^0\Lambda$ reaction compared with experimental data [11]. The first and second numbers in each figure correspond to the π^- beam momentum P_π (MeV/c) and the πN center-of-mass (c.m.) energy W (MeV), respectively.

C. $\pi^- p \to \eta n$

The chiral quark model approach was first extended to the study of the reaction $\pi^- p \to \eta n$ near threshold in our previous work [43]. Due to incomplete partial wave analysis for the $n = 2$ shell resonances, and no considerations of the configuration mixing between $N(1535)S_{11}$ and $N(1650)S_{11}$, we only obtained preliminary results. In this work, by combining the study of the reaction $\pi^- p \to K^0\Lambda$, we present

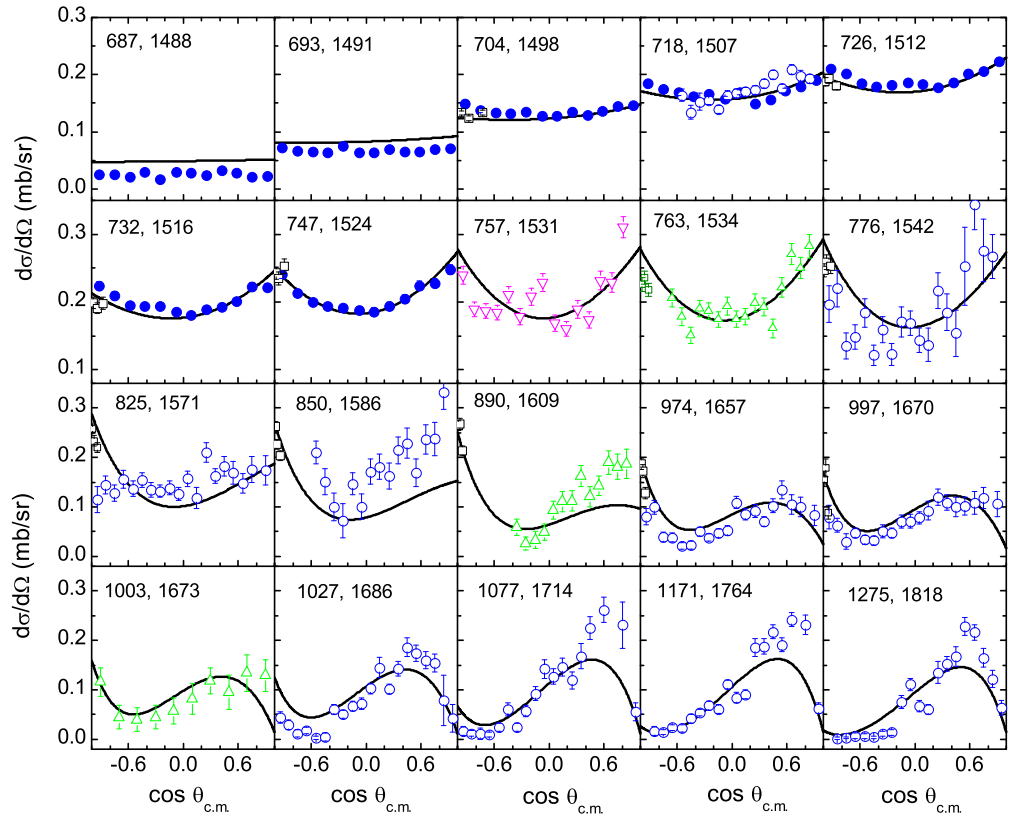

FIG. 5. Differential cross sections of the reaction $\pi^- p \to \eta n$ compared with the experimental data from Refs. [17] (open circle), [18] (open up-triangles), [19] (open down-triangles), [20] (open squares), and the recent experiment presented in Ref. [16] (solid circles). The first and second numbers in each figure correspond to the π^- beam momentum P_π (MeV/c) and the πN center-of-mass (c.m.) energy W (MeV), respectively.

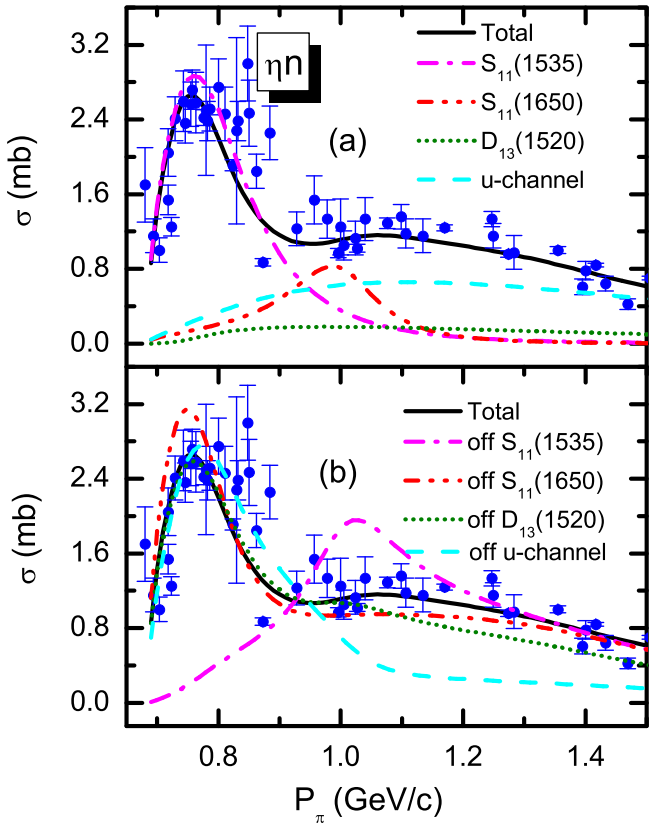

FIG. 6. Total cross section of the reaction $\pi^- p \to \eta n$ compared with experimental data [15]. The bold solid curves correspond to the full model result. In (a), exclusive cross sections for $S_{11}(1535)$, $S_{11}(1650)$, $N(1520)D_{13}$, and the u channel are indicated explicitly by the legends. In (b), the results by switching off the contributions of $S_{11}(1535)$, $S_{11}(1650)$, $N(1520)D_{13}$, and the u channel are indicated explicitly by the legends.

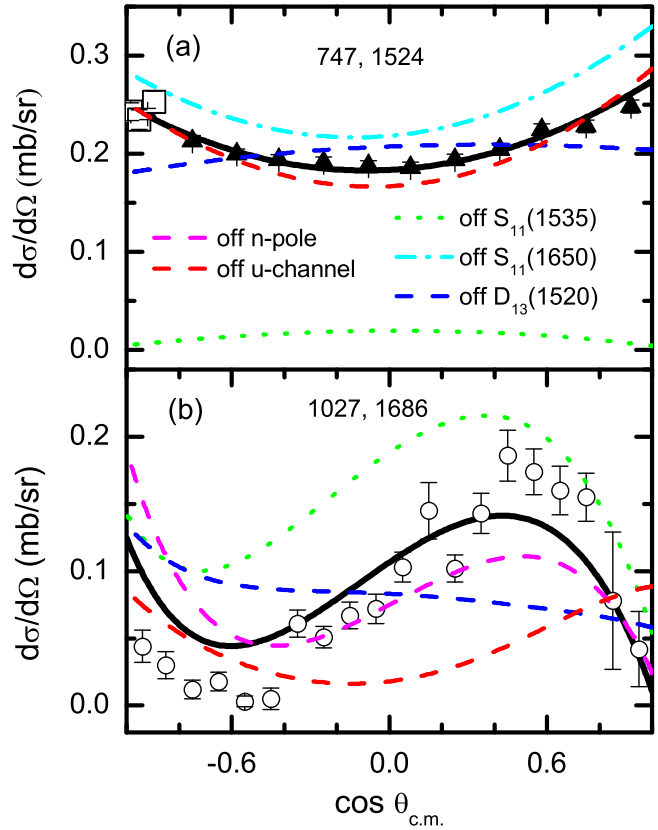

FIG. 7. Differential cross sections of the reaction $\pi^- p \to \eta n$ compared with experimental data at two energy points $P_\pi = 747, 1027$ MeV/c. The bold solid curves correspond to the full model result. The predictions by switching off the contributions from $N(1535)S_{11}$, $N(1650)S_{11}$, $N(1520)D_{13}$, and the n-pole and u-channel backgrounds are indicated explicitly by the legend in the figures.

a comprehensive study of the $\pi^- p \to \eta n$ process to better understand this reaction and extract more reliable properties of nucleon resonances.

The differential cross sections and total cross section compared with the experimental data are shown in Figs. 5 and 6, respectively. From the figures, it is seen that the experimental data in the c.m. energy range from threshold up to $W \simeq 1.8$ GeV can be reasonably described within the chiral quark model. Compared with our previous study in [43], the results in the present work have an obvious improvement.

In the S-wave states, the dominant role of $N(1535)S_{11}$ can be found in the reaction. It is responsible for the first hump around $P_\pi \simeq 0.76$ GeV/c ($W \simeq 1.5$ GeV). Without the $N(1535)S_{11}$ contribution, the first hump disappears completely. In addition, a sizable contribution from $N(1650)S_{11}$ can be seen from Figs. 6 and 7. Around the first hump, $N(1650)S_{11}$ has obvious destructive interferences with $N(1535)S_{11}$, which is consistent with our previous study [43]. In the total cross section there seems to exist another small bump structure around $P_\pi \simeq 1.0$ GeV/c ($W \simeq 1.7$ GeV). Based on our calculations shown in Fig. 6, the interferences between $N(1650)S_{11}$, $N(1535)S_{11}$, and u-channel background might be responsible for the this structure, which is different from our previous prediction [43]. Our results in present work are consistent with the those analyses within the coupled-channel approaches [27,32,40,41].

In the D-wave states, $N(1520)D_{13}$ plays an important role in the reaction, which can be obviously seen in the differential cross sections. Its interferences with the $N(1535)S_{11}$ and backgrounds are crucial to produce the correct shape of the differential cross sections in the whole energy region what we have considered. From Fig. 5 one can see that, without the $N(1520)D_{13}$ contribution, the shape of the differential cross sections changes significantly. However, no obvious effects of $N(1520)D_{13}$ on the total cross section can be found in the $\pi^- p \to \eta n$ reaction. This feature was mentioned in Refs. [35,36]. It should be pointed out that, to describe the data well, a large amplitude of $N(1520)D_{13}$ in the reaction is needed, which is about a factor of 2.18 larger than that derived in the SU(6)⊗O(3) limit, which cannot be explained with configuration mixing effects.

With the energy increasing, the u-channel background becomes more and more important in the reaction. Its large effects on both total cross section and differential cross sections can be notably seen in the energy region $P_\pi > 0.8$ GeV/c ($W > 1.5$ GeV). Its interferences with the resonances $N(1650)S_{11}$ and

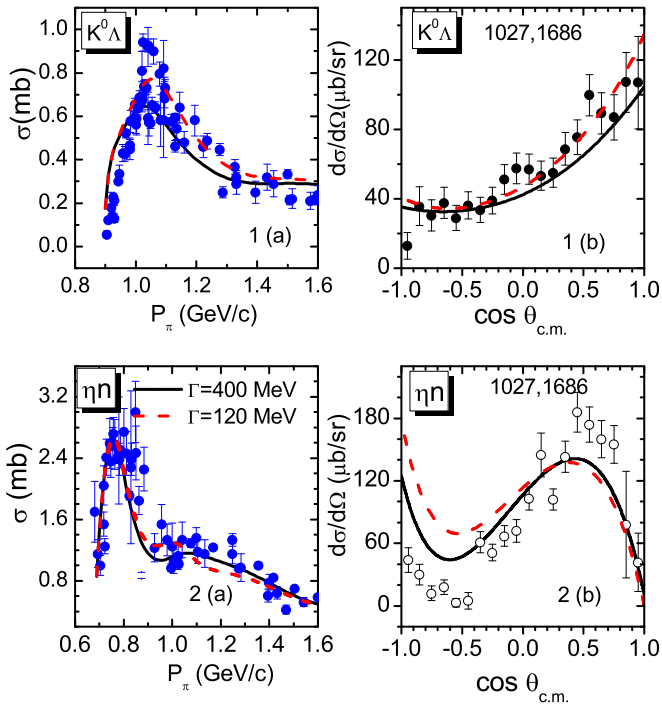

FIG. 8. Predictions for the $\pi^- p \to K^0\Lambda$ and ηn reactions with a narrow width $\Gamma = 120$ MeV and a broad width $\Gamma = 400$ MeV, respectively, for the resonance $N(1720)P_{13}$. The total cross sections for $\pi^- p \to K^0\Lambda$ and ηn are plotted in 1(a) and 2(a), respectively. While the differential cross sections at $P_\pi = 1027$ MeV/c for $\pi^- p \to K^0\Lambda$ and ηn are plotted in 1(b) and 2(b), respectively. The solid curves stand for the results with a broad width $\Gamma = 400$ MeV, while the dashed curves for the results with a narrow width $\Gamma = 120$ MeV.

$N(1535)S_{11}$ are responsible for the second bump structure around $P_\pi \simeq 1.0$ GeV/c ($W \simeq 1.7$ GeV).

No determined evidence of the other resonances, such as $D(1700)D_{13}$, $D(1675)D_{13}$, and higher P- and F-wave resonances, is found in the reaction. The background contributions from the n pole and t channel are less important to the reaction.

We should point out that some analyses of this reaction suggest the need of the $N(1710)P_{11}$ resonance [7,27,29,33]. However, according to our analysis, no obvious $N(1710)P_{11}$ contribution is required for a good description of the experimental observations. Meanwhile, our analysis indicates that $N(1720)P_{13}$ might have some effects on the cross sections. According to our results from partial wave analysis (see Table II), in the SU(6)⊗O(3) symmetry limit the scattering amplitudes of $N(1720)P_{13}$ are much larger than those of $N(1710)P_{11}$ around $W = 1.7$ GeV. Thus, the role of $N(1720)P_{13}$ might be more obvious than that of $N(1710)P_{11}$ if they are indeed seen in the reaction, which is consistent with the chiral quark model study in Ref. [44]. In this work, we find that the role of $N(1720)P_{13}$ is sensitive to its width (see Fig. 8). If we adopt a broad width of $\Gamma \simeq 400$ MeV obtained by fitting the data, the contributions of $N(1720)P_{13}$ to the reaction are negligibly small. However, if we adopt a narrower width $\Gamma \simeq 120$ MeV as suggested in our previous work by a study of the π^0 photoproduction [49]. From Fig. 8, we find that the second bump structure in the total cross section become more obvious, while around $W = 1.7$ GeV the cross sections at backward angles are enhanced significantly. It should be emphasized that, although our theoretical results seem to become bad compared with the data with a narrow width of $N(1720)P_{13}$, we cannot exclude this possibility because the old data obtained many years ago might be problematic due to uncontrollable uncertainties [23]. New observations of the $\pi^- p \to \eta n$ reaction are urgently needed to better understand the properties of nucleon resonances.

In brief, $N(1535)S_{11}$ plays a dominant role in the $\pi^- p \to \eta n$ reaction near the η production threshold. In this low energy region, $N(1650)S_{11}$ has a strong destructive interference with $N(1535)S_{11}$. The u-channel background also plays a crucial role in the reaction. The interferences between $N(1650)S_{11}$ and the u-channel background might be responsible for the second bump structure around $P_\pi \simeq 1.0$ GeV/c ($W \simeq 1.7$ GeV). $N(1520)D_{13}$ is crucial to describe the differential cross sections, although it has small contributions to the total cross section. To confirm the role of $N(1720)P_{13}$ in the reaction, new accurate measurements are urgently needed in the c.m. energy range $W \simeq 1.5$–1.8 GeV. No obvious evidence of $N(1700)D_{13}$, $N(1675)D_{15}$, $N(1710)P_{11}$, and $N(1680)F_{15}$ are found in the $\pi^- p \to \eta n$ reaction, which is in disagreement with the predictions in [7,27,29,33], where the authors predicted the $N(1710)P_{11}$ resonance is needed to explain the reaction.

D. Isospin-$\frac{1}{2}$ resonance contributions to πN scatterings

In this paper, from the $\pi^- p \to \eta n, K^0\Lambda$ reactions we have obtained a reasonable constraint of the isospin-$\frac{1}{2}$ resonance contributions to these reactions. According to the SU(6)⊗O(3) symmetry, we can further predict the s-channel isospin-$\frac{1}{2}$ resonance contributions to the $\pi N \to \pi N$ reactions, which might be helpful to better understand the $\pi N \to \pi N$ reactions.

By decomposing the initial and final isospin states of the πN system into linear combinations of s-channel isospin eigenstates, one can obtain the the relations between the πN isospin amplitudes [82]:

$$A(\pi^- p \to \pi^- p) = A(\pi^- n \to \pi^- n) = +\frac{1}{3}(2A^{1/2} + A^{3/2}), \tag{16}$$

$$A(\pi^- p \to \pi^0 n) = A(\pi^+ n \to \pi^0 p) = -\frac{\sqrt{2}}{3}(A^{1/2} - A^{3/2}), \tag{17}$$

$$A(\pi^0 n \to \pi^0 n) = A(\pi^0 p \to \pi^0 p) = +\frac{1}{3}(A^{1/2} + 2A^{3/2}), \tag{18}$$

where $A^{1/2}$ and $A^{3/2}$ correspond to the isospin-$\frac{1}{2}$ and $\frac{3}{2}$ resonance contributions, respectively. The isospin-$\frac{1}{2}$ resonance amplitudes $A^{1/2}$ for the $\pi N \to \pi N$ reactions can be related to the those listed in Table II for the $\pi^- p \to \eta n, K^0\Lambda$ reactions one by one according to the SU(6)⊗O(3) symmetry. Finally, we obtain the s-channel isospin-$\frac{1}{2}$ resonance contributions to the cross sections of the $\pi N \to \pi N$ reactions; our results are shown in Fig. 9. For comparison, the results of the $\pi^- p \to \eta n, K^0\Lambda$ reactions are also shown in the figure.

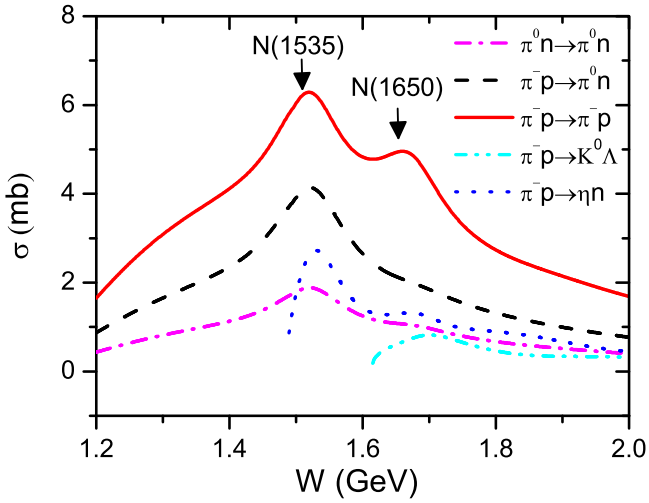

FIG. 9. The predictions of s-channel isospin-$\frac{1}{2}$ resonance contributions to the cross sections of the $\pi N \to \pi N$ reactions. For comparison, the results of the $\pi^- p \to \eta n, K^0\Lambda$ reactions are also shown.

From the figure, we can see that the s-channel isospin-$\frac{1}{2}$ resonance contributions to the $\pi^- p \to \pi^- p, \pi^0 n$ reactions are notably larger than those to the $\pi^- p \to \eta n, K^0\Lambda$ reactions. The s-channel isospin-$\frac{1}{2}$ resonance contributions to the $\pi^0 n \to \pi^0 n$ reaction are comparable to those to the $\pi^- p \to \eta n, K^0\Lambda$ reactions. Furthermore, from the figure it is found that the $N(1535)S_{11}$ resonance has obvious contributions to the πN reactions. The $N(1650)S_{11}$ resonance also contributes to the $\pi^- p \to \pi^- p$ reaction notably. Around the mass threshold of $N(1535)S_{11}$, we predict that

$$\frac{\sigma(\pi^- p \to \pi^- p)}{\sigma(\pi^- p \to \eta n)} \simeq 2.4, \quad \frac{\sigma(\pi^- p \to \pi^0 n)}{\sigma(\pi^- p \to \eta n)} \simeq 1.5, \quad \frac{\sigma(\pi^0 n \to \pi^0 n)}{\sigma(\pi^- p \to \eta n)} \simeq 0.7. \tag{19}$$

Further detailed analyses of the $\pi N \to \pi N$ reactions around the resonance energy region will be given in another work.

IV. SUMMARY

In this work, a combined study of the $\pi^- p \to K^0\Lambda$ and ηn reactions was carried out within a chiral quark model. We have achieved reasonable descriptions of the data in the c.m. energy range from threshold up to $W \simeq 1.8$ GeV.

Obvious evidence of the S-wave nucleon resonances $N(1535)S_{11}$ and $N(1650)S_{11}$ is found in both of these reactions. $N(1650)S_{11}$ contributes to the $\pi^- p \to K^0\Lambda$ reaction through configuration mixing with $N(1535)S_{11}$. The determined mixing angle is $\theta_s \simeq 26.9^\circ$, which is consistent with that extracted from η and π^0 photoproduction processes in our previous works [48,49]. Furthermore, the partial width ratios $\Gamma_{\eta N}/\Gamma_{\pi N}$ and $\Gamma_{K\Lambda}/\Gamma_{\pi N}$ for these S-wave states are extracted from the reactions, which are close to the upper limit of the average values from the PDG [2]. An obvious role of the D-wave state $N(1520)D_{13}$ is found in the $\pi^- p \to \eta n$ reaction, which has large effects on the differential cross sections although its effects on the total cross section are tiny. It should be pointed out that the effects of $N(1520)D_{13}$ on the $\pi^- p \to K^0\Lambda$ reaction are negligibly small.

The backgrounds play remarkable roles in these two strong interaction processes. In the $\pi^- p \to K^0\Lambda$ process, the u-, t-channel, and n-pole backgrounds have notable contributions to the cross sections. In the $\pi^- p \to \eta n$ process, the u-channel background plays a crucial role in the higher energy region $W > 1.5$ GeV.

The role of $N(1720)P_{13}$ should be further confirmed by future experiments. In the present work, the data seem to favor a broad width $\Gamma > 200$ MeV for $N(1720)P_{13}$. However, our previous study of the π^0 photoproduction process indicates that the $N(1720)P_{13}$ might have a narrow width of $\Gamma \simeq 120$ MeV [49]. If $N(1720)P_{13}$ has a broad width of $\Gamma \simeq 400$ MeV, its contributions to the reactions $\pi^- p \to K^0\Lambda$ and ηn should be negligibly small. However, if $N(1720)P_{13}$ has a narrow width of $\Gamma \simeq 120$ MeV, its contributions to the reactions are obvious, which can be seen from both the total cross section and differential cross sections. The present data of the $\pi^- p \to K^0\Lambda$ allow the appearance of a narrow $N(1720)P_{13}$ resonance within the uncertainties. However, when using a narrow width of $N(1720)P_{13}$ in the $\pi^- p \to \eta n$ reaction, our theoretical results are notably larger than the data at the backward angles. Improved measurements and more reliable experimental data of the $\pi^- p \to K^0\Lambda$ and ηn reactions are needed to clarify the puzzle about $N(1720)P_{13}$.

It should be pointed out that no obvious evidence of $N(1700)D_{13}$, $N(1675)D_{15}$, $N(1710)P_{11}$, and $N(1680)F_{15}$ was found in the $\pi^- p \to K^0\Lambda$ and ηn reactions, although they lie in the energy range that we considered.

Finally, according to the SU(6)⊗O(3) symmetry, we further predict the s-channel isospin-$\frac{1}{2}$ resonance contributions to the $\pi N \to \pi N$ reactions, which might be helpful to better understand the $\pi N \to \pi N$ reactions.

ACKNOWLEDGMENTS

This work is partly supported by the National Natural Science Foundation of China (Grants No. 11075051 and No. 11375061), the Hunan Provincial Natural Science Foundation (Grant No. 13JJ1018), and the Hunan Provincial Innovation Foundation for Postgraduate.

[1] E. Klempt and J. M. Richard, Baryon spectroscopy, Rev. Mod. Phys. **82**, 1095 (2010).
[2] K. A. Olive *et al.* (Particle Data Group Collaboration), Review of particle physics, Chin. Phys. C **38**, 090001 (2014).
[3] N. Isgur and G. Karl, P wave baryons in the quark model, Phys. Rev. D **18**, 4187 (1978).
[4] N. Isgur and G. Karl, Hyperfine interactions in negative parity baryons, Phys. Lett. B **72**, 109 (1977); Positive-parity excited baryons in a quark model with hyperfine interactions, Phys.

Rev. D **19**, 2653 (1979); N. Isgur, Erratum: Two-photon decay of the pseudoscalar mesons, *ibid.* **23**, 817 (1981); N. Isgur and G. Karl, Ground state baryons in a quark model with hyperfine interactions, *ibid.* **20**, 1191 (1979).

[5] S. Capstick and N. Isgur, Baryons in a relativized quark model with chromodynamics, Phys. Rev. D **34**, 2809 (1986).

[6] W. J. Briscoe, M. Döring, H. Haberzettl, D. M. Manley, M. Naruki, I. I. Strakovsky, and E. S. Swanson, Physics opportunities with meson beams, Eur. Phys. J. A **51**, 129 (2015).

[7] D. Ronchen *et al.*, Coupled-channel dynamics in the reactions $\pi N \to \pi N, \eta N, K\Lambda, K\Sigma$, Eur. Phys. J. A **49**, 44 (2013).

[8] L. Bertanza, P. L. Connolly, B. B. Culwick, F. R. Eisler, T. Morris, R. B. Palmer, A. Prodell, and N. P. Samios, ΛK^0 Production by Pions on Protons, Phys. Rev. Lett. **8**, 332 (1962).

[9] J. J. Jones *et al.*, Total Cross-Sections for $\pi^- p \to \Lambda K^0$ from Threshold to 1.13 GeV/c, Phys. Rev. Lett. **26**, 860 (1971).

[10] T. M. Knasel *et al.*, Experimental study of the reaction $\pi^- p \to \Lambda K^0$ at beam momenta between 930 and 1130 MeV/c, Phys. Rev. D **11**, 1 (1975).

[11] R. D. Baker *et al.*, The Reaction $\pi^- p \to K^0 \Lambda^0$ up to 1334 MeV/c, Nucl. Phys. B **141**, 29 (1978).

[12] D. H. Saxon *et al.*, The reaction $\pi^- p \to K^0 \Lambda^0$ up to 2375 MeV/c: New results and analysis, Nucl. Phys. B **162**, 522 (1980).

[13] T. O. Binford, M. L. Good, V. G. Lind, D. Stern, R. Krauss, and E. Dettman, Production of Λ^0 and Σ^0 hyperons by pions of beam momenta 1.12–1.32 BeV/c, Phys. Rev. **183**, 1134 (1969).

[14] B. Nelson *et al.*, Search for Structure in $\pi^- p \to K^0 \Lambda^0$ at ΣK Threshold, Phys. Rev. Lett. **31**, 901 (1973).

[15] A. Baldini, V. Flaminio, W. G. Moorhead, D. R. O. Morrison, and H. Schopper, *Total Cross-sections For Reactions of High-energy Particles (Including Elastic, Topological, Inclusive and Exclusive Reactions)*, Landolt-Börnstein, New Series, Group 1, Vol. 12 (Springer, Berlin, 1988).

[16] S. Prakhov *et al.*, Measurement of $\pi^- p \to \eta n$ from threshold to $P_{\pi^-} = 747$ MeV/c, Phys. Rev. C **72**, 015203 (2005).

[17] R. M. Brown *et al.*, Differential cross-sections for the reaction $\pi^- p \to \eta n$ between 724 MeV/c and 2723 MeV/c, Nucl. Phys. B **153**, 89 (1979).

[18] W. Deinet, H. Mueller, D. Schmitt, H. M. Staudenmaier, S. Buniatov, and E. Zavattini, Differential and total cross-sections for $\pi^- p \to \eta n$ from 718 to 1050 MeV/c, Nucl. Phys. B **11**, 495 (1969).

[19] J. Feltesse, R. Ayed, P. Bareyre, P. Borgeaud, M. David, J. Ernwein, Y. Lemoigne, and G. Villet, The reaction $\pi^- p \to \eta n$ up to $P_\eta^* = 450$ MeV/c: Experimental results and partial wave analysis, Nucl. Phys. B **93**, 242 (1975).

[20] N. C. Debenham *et al.*, Backward $\pi^- p$ reactions between 0.6 GeV/c and 1 GeV/c, Phys. Rev. D **12**, 2545 (1975).

[21] F. Bulos *et al.*, Charge exchange and production of eta mesons and multiple neutral pions in $\pi^- p$ reactions between 654 and 1247 MeV/c, Phys. Rev. **187**, 1827 (1969).

[22] W. B. Richards *et al.*, Production and neutral decay of the η meson in $\pi^- p$ collisions, Phys. Rev. D **1**, 10 (1970).

[23] M. Clajus and B. M. K. Nefkens, The $\pi^- p \to \eta n$ database, PiN Newslett. **7**, 76 (1992).

[24] T. Hyodo, S. I. Nam, D. Jido, and A. Hosaka, Detailed analysis of the chiral unitary model for meson baryon scatterings with flavor SU(3) breaking effects, Prog. Theor. Phys. **112**, 73 (2004).

[25] M. Shrestha and D. M. Manley, Partial-wave analysis of $\pi^- p \to \eta n$ and $\pi^- p \to K^0 \Lambda$ reactions, Phys. Rev. C **86**, 045204 (2012).

[26] M. Shrestha and D. M. Manley, Multichannel parametrization of πN scattering amplitudes and extraction of resonance parameters, Phys. Rev. C **86**, 055203 (2012).

[27] G. Penner and U. Mosel, Vector meson production and nucleon resonance analysis in a coupled channel approach for energies $m_N < \sqrt{s} < 2$ GeV. I: Pion induced results and hadronic parameters, Phys. Rev. C **66**, 055211 (2002).

[28] V. Shklyar, H. Lenske, and U. Mosel, A coupled-channel analysis of $K\Lambda$ production in the nucleon resonance region, Phys. Rev. C **72**, 015210 (2005).

[29] V. Shklyar, H. Lenske, and U. Mosel, η-meson production in the resonance-energy region, Phys. Rev. C **87**, 015201 (2013).

[30] M. Sotona and J. Zofka, Elementary amplitudes of the process $\pi^- p \to K^0 \Lambda$, Prog. Theor. Phys. **81**, 160 (1989).

[31] T. Feuster and U. Mosel, A unitary model for meson-nucleon scattering, Phys. Rev. C **58**, 457 (1998).

[32] V. Shklyar, G. Penner, and U. Mosel, Spin 5/2 resonance contributions to the pion induced reactions for energies $\sqrt{s} \leqslant$ 2.0 GeV, Eur. Phys. J. A **21**, 445 (2004).

[33] V. Shklyar, H. Lenske, and U. Mosel, η-photoproduction in the resonance energy region, Phys. Lett. B **650**, 172 (2007).

[34] R. A. Arndt, W. J. Briscoe, I. I. Strakovsky, R. L. Workman, and M. M. Pavan, Dispersion relation constrained partial wave analysis of πN elastic and $\pi N \to \eta N$ scattering data: The baryon spectrum, Phys. Rev. C **69**, 035213 (2004).

[35] R. A. Arndt, W. J. Briscoe, T. W. Morrison, I. I. Strakovsky, R. L. Workman, and A. B. Gridnev, Low-energy η-N interactions: Scattering lengths and resonance parameters, Phys. Rev. C **72**, 045202 (2005).

[36] A. M. Gasparyan, J. Haidenbauer, C. Hanhart, and J. Speth, Pion-nucleon scattering in a meson-exchange model, Phys. Rev. C **68**, 045207 (2003).

[37] B. Julia-Diaz, B. Saghai, T.-S. H. Lee, and F. Tabakin, Dynamical coupled-channels approach to hadronic and electromagnetic kaon-hyperon production on the proton, Phys. Rev. C **73**, 055204 (2006).

[38] W. T. Chiang, B. Saghai, F. Tabakin and T. S. H. Lee, Dynamical coupled-channel model of kaon-hyperon interactions, Phys. Rev. C **69**, 065208 (2004).

[39] T. P. Vrana, S. A. Dytman, and T. S. H. Lee, Baryon resonance extraction from πN data using a unitary multichannel model, Phys. Rep. **328**, 181 (2000).

[40] J. Durand, B. Julia-Diaz, T.-S. H. Lee, B. Saghai, and T. Sato, Insights into the $\pi^- p \to \eta n$ reaction mechanism, Int. J. Mod. Phys. A **24**, 553 (2009).

[41] J. Durand, B. Julia-Diaz, T.-S. H. Lee, B. Saghai, and T. Sato, Coupled-channels study of the $\pi^- p \to \eta n$ process, Phys. Rev. C **78**, 025204 (2008).

[42] A. V. Anisovich, R. Beck, E. Klempt, V. A. Nikonov, A. V. Sarantsev, U. Thoma, and Y. Wunderlich, Study of ambiguities in $\pi^- p \to \Lambda K^0$ scattering amplitudes, Eur. Phys. J. A **49**, 121 (2013).

[43] X. H. Zhong, Q. Zhao, J. He, and B. Saghai, Study of $\pi^- p \to \eta n$ at low energies in a chiral constituent quark model, Phys. Rev. C **76**, 065205 (2007).

[44] J. He and B. Saghai, Combined study of $\gamma p \to \eta p$ and $\pi^- p \to \eta n$ in a chiral constituent quark approach, Phys. Rev. C **80**, 015207 (2009).

[45] C. Z. Wu, Q. F. Lü, J. J. Xie, and X. R. Chen, Nucleon resonances in the $\pi^- p \to K^0 \Lambda$ reaction near threshold, Commun. Theor. Phys. **63**, 215 (2015).

[46] Q.-F. Lü, X.-H. Liu, J.-J. Xie, and D.-M. Li, The near threshold $\pi^- p \to \eta n$ reaction in an effective Lagrangian approach, Mod. Phys. Lett. A **29**, 1450012 (2014).

[47] S. Ceci, A. Svarc, and B. Zauner, The re-analysis of the 1700-MeV structure of the P_{11} partial wave using the $\pi N \to K\Lambda$ production data, Few Body Syst. **39**, 27 (2006).

[48] X. H. Zhong and Q. Zhao, η photoproduction on the quasifree nucleons in the chiral quark model, Phys. Rev. C **84**, 045207 (2011).

[49] L. Y. Xiao, X. Cao, and X. H. Zhong, Neutral pion photoproduction on the nucleon in a chiral quark model, Phys. Rev. C **92**, 035202 (2015).

[50] B. C. Liu and B. S. Zou, Mass and $K\Lambda$ Coupling of $N^*(1535)$, Phys. Rev. Lett. **96**, 042002 (2006).

[51] B. S. Zou, Strangeness in the proton and $N^*(1535)$, Nucl. Phys. A **790**, 110 (2007).

[52] L. S. Geng, E. Oset, B. S. Zou, and M. Doring, Role of the $N^*(1535)$ in the $J/\psi \to \bar{p}\eta p$ and $J/\psi \to \bar{p}K^+\Lambda$ reactions, Phys. Rev. C **79**, 025203 (2009).

[53] T. Inoue, E. Oset, and M. J. Vicente Vacas, Chiral unitary approach to S-wave meson-baryon scattering in the strangeness $S = 0$ sector, Phys. Rev. C **65**, 035204 (2002).

[54] J. Nieves and E. Ruiz Arriola, S_{11}-$N(1535)$ and -$N(1650)$ resonances in meson-baryon unitarized coupled channel chiral perturbation theory, Phys. Rev. D **64**, 116008 (2001).

[55] M. Doring and K. Nakayama, The phase and pole structure of the $N^*(1535)$ in $\pi N \to \pi N$ and $\gamma N \to \pi N$, Eur. Phys. J. A **43**, 83 (2010).

[56] Z. P. Li, Threshold pion photoproduction of nucleons in the chiral quark model, Phys. Rev. D **50**, 5639 (1994).

[57] Z. P. Li, Kaon photoproduction of nucleons in the chiral quark model, Phys. Rev. C **52**, 1648 (1995).

[58] Z. P. Li, η photoproduction of nucleons and the structure of the resonance $S_{11}(1535)$ in the quark model, Phys. Rev. D **52**, 4961 (1995).

[59] Z. P. Li, H. X. Ye, and M. H. Lu, Unified approach to pseudoscalar meson photoproductions off nucleons in the quark model, Phys. Rev. C **56**, 1099 (1997).

[60] Q. Zhao, J. S. Al-Khalili, Z. P. Li, and R. L. Workman, Pion photoproduction on the nucleon in the quark model, Phys. Rev. C **65**, 065204 (2002).

[61] Q. Zhao, Z. P. Li, and C. Bennhold, Vector meson photoproduction with an effective Lagrangian in the quark model, Phys. Rev. C **58**, 2393 (1998).

[62] Q. Zhao, J. S. Al-Khalili, and C. Bennhold, Quark model predictions for K^* photoproduction on the proton, Phys. Rev. C **64**, 052201 (2001).

[63] Q. Zhao, Z. P. Li, and C. Bennhold, Ω and ρ photoproduction with an effective quark model Lagrangian, Phys. Lett. B **436**, 42 (1998).

[64] Z. P. Li and B. Saghai, Study of the baryon resonances structure via η photoproduction, Nucl. Phys. A **644**, 345 (1998).

[65] B. Saghai and Z. P. Li, Quark model study of the η photoproduction: Evidence for a new S_{11} resonance?, Eur. Phys. J. A **11**, 217 (2001).

[66] Q. Zhao, B. Saghai, and Z. P. Li, Quark model approach to the η meson electroproduction on the proton, J. Phys. G **28**, 1293 (2002).

[67] J. He, B. Saghai, and Z. P. Li, Study of η photoproduction on the proton in a chiral constituent quark approach via one-gluon-exchange model, Phys. Rev. C **78**, 035204 (2008).

[68] X. H. Zhong and Q. Zhao, η' photoproduction on the nucleons in the quark model, Phys. Rev. C **84**, 065204 (2011).

[69] L. Y. Xiao and X. H. Zhong, Low-energy $K^- p \to \Lambda\eta$ reaction and the negative parity Λ resonances, Phys. Rev. C **88**, 065201 (2013).

[70] X. H. Zhong and Q. Zhao, The $K^- p \to \Sigma^0\pi^0$ reaction at low energies in a chiral quark model, Phys. Rev. C **79**, 045202 (2009).

[71] X. H. Zhong and Q. Zhao, Low energy reactions $K^- p \to \Sigma^0\pi^0$, $\Lambda\pi^0$, $\bar{K}^0 n$ and the strangeness $S = -1$ hyperons, Phys. Rev. C **88**, 015208 (2013).

[72] J. Hamilton and W. S. Woolcock, Determination of pion-nucleon parameters and phase shifts by dispersion relations, Rev. Mod. Phys. **35**, 737 (1963).

[73] R. G. Moorhouse, Photoproduction of N^* Resonances in the Quark Model, Phys. Rev. Lett. **16**, 772 (1966).

[74] Q. Zhao and F. E. Close, Quarks, diquarks and QCD mixing in the N^* resonance spectrum, Phys. Rev. D **74**, 094014 (2006).

[75] M. L. Goldberger and S. B. Treiman, Decay of the π meson, Phys. Rev. **110**, 1178 (1958).

[76] J. Piekarewicz, Off-shell behavior of the π-η mixing amplitude, Phys. Rev. C **48**, 1555 (1993).

[77] L. Tiator, C. Bennhold, and S. S. Kamalov, The ηNN coupling in η photoproduction, Nucl. Phys. A **580**, 455 (1994).

[78] S. L. Zhu, The ηNN coupling constant, Phys. Rev. C **61**, 065205 (2000).

[79] W. T. Chiang, F. Tabakin, T. S. H. Lee, and B. Saghai, Coupled channel study of $\gamma p \to K^+\Lambda$, Phys. Lett. B **517**, 101 (2001).

[80] O. Krehl, C. Hanhart, S. Krewald, and J. Speth, What is the structure of the Roper resonance?, Phys. Rev. C **62**, 025207 (2000).

[81] M. Ripani *et al.* (CLAS Collaboration), Measurement of $ep \to e' p\pi^+\pi^-$ and Baryon Resonance Analysis, Phys. Rev. Lett. **91**, 022002 (2003).

[82] C. Ditsche, M. Hoferichter, B. Kubis, and U.-G. Meissner, Roy-Steiner equations for pion-nucleon scattering, J. High Energy Phys. 06 (2012) 043.